Full Facility Shock Frame Simulations
of the Electric Arc Shock Tube

Durgesh Chandel*
University of Minnesota, Minneapolis, MN, 55455

Aaron Brandis[†]
AMA Inc. at NASA Ames, Mountain View, CA, 94035, USA

Graham V. Candler[‡]
University of Minnesota, Minneapolis, MN, 55455

Radiative heating computations are performed for high speed lunar return experiments conducted in the Electric Arc Shock Tube (EAST) facility at NASA Ames Research Center. The nonequilibrium radiative transport equations are solved via NASA's in-house radiation code NEQAIR using flow field input from US3D flow solver. The post-shock flow properties for the 10 km/s Earth entry conditions are computed using the stagnation line of a blunt-body and a full facility CFD simulation of the EAST shock tube. The shocked gas in the blunt-body flow achieves a thermochemical equilibrium away from the shock front whereas EAST flow exhibits a nonequilibrium behavior due to strong viscous dissipation of the shock by boundary layer. The full-tube flow calculations capture the influence of the boundary layer on the shocked gas state and provide a realistic fluid dynamic input for the radiative predictions. The integrated radiance behind the shock is calculated in NEQAIR for wavelength regimes from Vacuum-UltraViolet (VUV) to InfraRed (IR), which are pertinent to the emission characteristics of high enthalpy shock waves in air. These radiance profiles are validated against corresponding EAST shots. The full-tube simulations successfully predict a sharp radiance peak at the shock front which gets smeared in the test data due to the spatial resolution in the measurements. The full facility based radiance behind the shock shows a slightly better match with the test data in the VUV and Red spectral regions, as compared to that from a blunt-body based predictions. The UV radiance is very similar for both geometries and under-predicts the test behavior. The IR test data matches better with the blunt-body based predictions where the full-tube simulations show a significant over-prediction.

I. Introduction

The survival of a space vehicle during an atmospheric entry heavily relies on the performance of its Thermal Protection System (TPS). The Electric Arc Shock Tube (EAST) facility at NASA Ames Research Center has been extensively used to reproduce strong shock waves for a range of atmospheric entry conditions in order to provide heating estimates for TPS design and validation support. The spectroscopic data gathered in EAST experiments can be used to inform the CFD models and validate in-flight measurements but a complete understanding of the shocked gas behavior solely through experiments is challenging. Given the limitations and uncertainties in the measurement, companion CFD simulations of the test facility are required to gain a deeper insight of the flow physics. For this reason, the EAST radiation data has been interpreted using high-fidelity numerical predictions of the flow and radiation properties of the shocked gas using a stagnation line of a blunt-body geometry at appropriate conditions.

Recently, Brandis *et al.* [1] performed radiative heating validation studies for Earth entry shocks at speeds from 9.5 to 15.5 km/s. The radiance predictions using a blunt-body flow field led to some differences in the VUV (145 - 195 nm) and UV (330 - 490 nm) spectral regions and the overall radiative predictions showed significant deviation from the test data at Earth entry speeds less than 10 km/s. Additionally, the backshell radiation studies pertinent to Earth and Mars high speed entry conditions were performed by West *et al.* [2], Brandis *et al.* [3], Johnston & Brandis [4], etc., which highlighted two key aspects: (a) the shock-heated gas exhibits a state of strong thermochemical nonequilibrium, and (b) the radiative heating component can be equal or higher than convective heating at certain conditions (e.g., Earth entry speeds higher than 10 km/s). Thus, an optimal TPS design requires accurate predictions of both the compressive

shocked flow behavior on the frontside of the space vehicle and the expanding shocked flow properties near the backshell. Furthermore, the expanding shocked flow experiments in the shock tubes demand for a full facility based prediction of the gas state to accurately estimate the test start- and end-times based on the arrival of the shock and expansion waves. Therefore, the high-fidelity characterization of the full EAST facility is sought after.

The radiative behavior of a gas is governed by its local thermochemical state, i.e., the concentrations of various species present in the gaseous mixture and the energy distributed among different modes. The high enthalpy flow in EAST shock tube exhibits a variety of strongly coupled thermochemical processes over a large range of length- and time-scales, which makes numerical computations challenging. Moreover, as the shock wave propagates downstream, it generates a thin boundary layer which exhibits a high viscous shearing, causing a significant deceleration of the shock front and curving its shape in the near-wall region. Since the speed of the shock wave directly governs the post-shock equilibrium state, a decelerating shock front will compress the test gas with reducing strength, i.e., the post-shock equilibrium temperatures reduce as the shock front travels along the tube. Furthermore, the boundary layer is relatively cold as compared to the main flow and contains higher fractions of neutralized ions and recombined molecular species, such as N, O, NO, etc., resulting in additional radiative absorption at the wall. Thus, for a realistic prediction of the radiative signature of the gas at the EAST test section, an accurate fluid dynamic solution is required that closely captures the influence of the boundary layer on the shocked gas for the entire duration of shock propagation.

Brandis *et al.* [5] simulated the effects of shock deceleration in 1-D NEQAIR calculations where the shock deceleration profile was calculated based on the measured shock arrival time at different axial locations along the tube. The inclusion of shock deceleration improved the agreement to the experimental data. It is evident that the boundary layer growing at the wall has a significant impact on the properties of the shocked gas, and therefore, modeling a 2-D axisymmetric EAST shock tube flow is necessary to get a more complete and realistic understanding of the flow physics.

Researchers have attempted time-accurate, full-facility-based CFD simulations of EAST flow. Kotov *et al.* [6] simulated EAST flow in a 2D channel using a simplified single-temperature energy model with explicit time-integration methods. These simulations incurred a significant computational cost and suffered from spurious oscillations near the contact front. Therefore, an accurate representation of the flow field at the test section could not be obtained. Since full-facility CFD simulations were not available, radiation predictions for EAST use the flow field from a simplified approach, i.e., computing a blunt-body problem with the LAURA or DPLR fluid solvers, where the shock speed and the shock stand-off distance were appropriately chosen to correspond to the measurements at the test section. Computations of the post-shock flow field with this approach are inexpensive but neglect the actual evolution of the shocked flow, leading to significant deviations from the experimental data under certain conditions. Cruden [7] found that the measured electron density in lunar Earth entry experiments at EAST were up to several times larger than equilibrium values to a significant distance behind the shock front. The discrepancy increases at lower entry speeds, $8 - 10$ km/s, suggesting that the shock deceleration effects are stronger at these conditions and using a simple blunt-body flow field may not be appropriate. For example, the uncertainties in the radiative predictions were as high as 70% in NEQAIR and up to 60% in HARA for moderately high entry speeds [7].

In a recent effort by the authors [8, 9], physics based full facility EAST simulations were performed using an improvized methodology in the US3D flow solver. The numerical solution successfully captured the shock-boundary layer interaction in a computationally feasible manner, and predicted a shock deceleration that is of same order as observed in EAST.

The goal of the present work is to provide an accurate representation of the radiation field and associated heating in the post-shock region for 10 km/s Earth entry at 0.2 torr ambient pressure conditions. The next section highlights some aspects of the measurement process in the experiments, followed by a brief description of the computational tools used in this analysis. Since the radiative emission/absorbtion characteristics of the shock-heated gas are strongly related to the thermochemical evolution of the gas state, a full facility flow field [9] from US3D is used to perform the radiation calculations in NEQAIR. These radiative heating predictions are compared with the experimental data and also with the predicted radiation field when a simplified blunt body flow simulation was fed as an input. A summary of the important observations is presented, and the scope of the future work is discussed.

II. Experimental Facility

The operational envelope of EAST covers a huge range of interplanetary missions. A schematic of the Electric Arc Shock tube (EAST) is shown in Fig. 1. The high enthalpy shock waves are generated in a long, narrow tube with a diameter of 10.16 cm. The test section is located at about 8 m downstream of the primary diaphragm where the spectroscopic images of the shock are captured using four separate charge-coupled device (CCD) arrays for four different
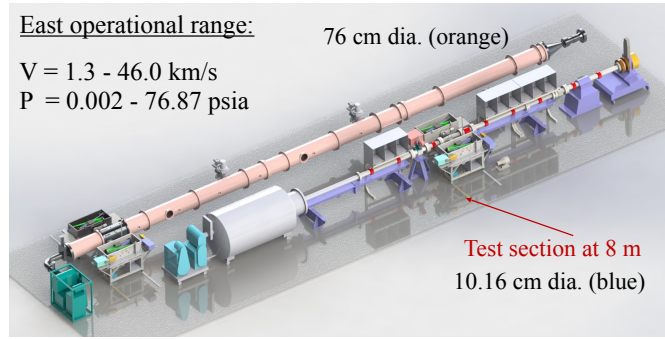
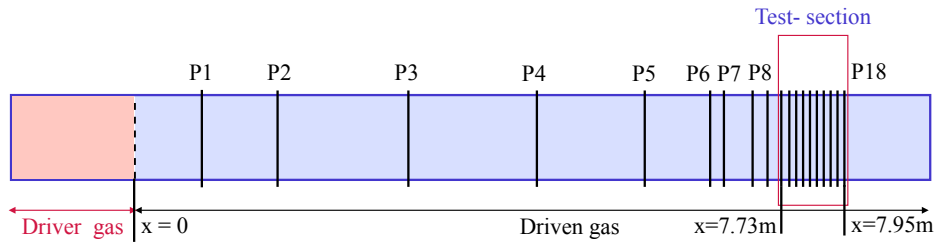**Fig. 1   Schematic of the EAST shock-tube Facility at NASA Ames**

Fig. 2   Pressure sensor locations along EAST shock tube

regimes of radiation spectra ranging from 120 nm to 1600 nm. The shock deceleration profile along the tube is estimated by recording the arrival times of shock through 18 pressure sensors placed on the tube walls. The shock arrival time is first reported after 1.06 m of shock travel at sensor P1. These sensors are distributed along the tube in a way such that more data is collected towards the test section, as shown in Fig. 2. Near the test section, pressure sensors P8 to P18 are located at every 3 cm of shock travel, providing a well-resolved data for the equilibrium shock speed calculations. A more detailed documentation on the instrumentation and measurement process can be found in Ref. [7, 10–12].

III. Computational Tools

The shock tube jump conditions in the present calculations correspond to the return trajectories from the moon at 10 km/s (0.2 Torr). As mentioned earlier, full shock tube CFD simulations of this strongly nonlinear flow with stiff source terms are prone to numerical instabilities developing in the boundary layer, which can feed back into the subsonic region behind the normal shock, leading to spurious shock speed predictions and/or distortion of the shock front. An attempt to mitigate these instabilties by resolving all important length and time scales of the problem can make the process computationally exhaustive.

With a systematic analysis, we devised a numerical framework to accurately solve such high-speed shock propagation problems. The time-accurate fluid dynamic simulations for a full facility EAST flow are obtained by solving the compressible Navier-Stokes equations in the shock-frame of reference using US3D, an unstructued three dimensional hypersonic compressible flow solver developed at the University of Minnesota. An implicit time-integration scheme is used in conjunction with the improvized numerics essential to obtain a stable and realistic flow solution. More details on this fluid solver methodology can be found in [8, 9]. This physics-based flow field is fed as an input to NEQAIR, which is NASA's in-house solver for NonEQuilibrium AIr Radiation. NEQAIR computes the spontaneous radiative properties of the gas along a line-of-sight specified in the direction normal to the shock-propagation. A tangent slab approximation is used to solve the radiative transport equations. The spontaneous emission, absorption and stimulated emission spectra are obtained for various species present in the gas mixture.
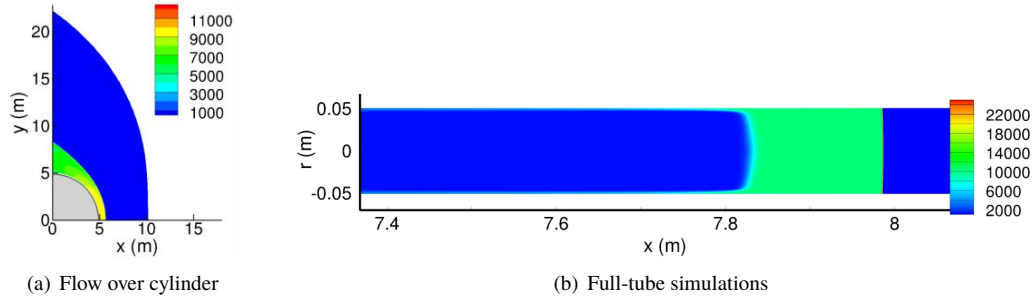
(a) Flow over cylinder   (b) Full-tube simulations

Fig. 3   Post-shock temperature field for 10 km/s shock

IV. Results and Discussion

As mentioned earlier, the flow field inputs greatly influence the quality of radiative predictions. The key features of the fluid solver results are presented in this section followed by an analysis of the numerically predicted radiance profiles.

A. CFD Predictions

The radiative calculations in the current study are performed using the post-shock gas state from a cylinder and a full-tube flow simulation for 10 km/s shock in air (79% N_2 + 21% O_2). The full-tube simulations use helium as a driver gas which is initially separated from the test gas by means of a thin aluminium diaphragm. The diaphragm rupture process is modeled to be instantaneous and uniform over the tube cross-section. The cylinder flow simulations use a quarter-cylinder geometry with a big nose radius of 5 m. This ensures a large shock stand-off distance of about 60 cm and a 15-20 cm wide post-shock equilibrium region which is free from the wall effects. The full-tube simulations are performed using a variable resolution grid in a moving frame of reference. Both these simulations use implicit time-integration schemes using a line-relaxation for the cylinder and point-relaxation for the tube geometry. The numerical fluxes are upwinded and an 11-species weakly ionzed air model is used with two-temperature CFD model. The transport properties come from collision-integral based models suitable for high temperature conditions behind the 10 km/s shock. More details on the numerical modeling can be found in Refs. [8, 9].

The fluid solver results for the cylinder and the tube flow at EAST test-section, are presented in Fig. 3. The centerline profiles from the tube flow are compared with the stagnation line and the CEA * equilibrium state (see Fig. 4). The post-shock gas in the cylinder flow has significantly lower temperatures in the nonequilibrium region near the shock front. Moreover, the equilibrium region for the cylinder flow reaches close to a CEA equilibrium state, whereas the full-tube simulations show slowly increasing temperatures and electron density towards the contact front. This is due to the nonequilibrium effects caused by the interaction of the shock with the boundary layer. An important observation here is that the tube flow gas state just behind the shock front has converged to a non-CEA level; the equilibrium gas temperatures and electron density just behind the shock are about 10,350 K and 1.1E+16 per cm^3 respectively as compared to CEA predicted values of about 9,890 K and 0.8E+16 per cm^3. This is hypothesized to be an artifact of the rapid axial stretching of the tube grid just after 2 cm behind the shock which needs to be investigated in future simulations. For the current puposes, it is known that the test gas shows increasing nonequilibrium effects towards the contact front, with gas temperatures and electron density being significantly higher than the equilibrium state just behind the shock front. The current full-tube simulations predict a similar trend, the gas state towards the contact front deviates from the non-CEA equilibrium achieved just behind the shock. The temperatures, electron density, etc., increase towards the contact front.

Since the full-tube simulations capture the boundary layer effects, it is interesting to analyze the radial variation of the key flow parameters and assess their impact on the radiative predictions. The radial data at various axial stations behind the shock are extracted from the full-tube simulations, labeled with (a) - (e) in Fig. 5. The radial profiles of the translational and vib.-electronic temperatures are plotted in Fig. 6. A strong nonequilibrium between the two energy modes can be seen in the vicinity of the shock front, e.g., at station (e). Going from right to left, i.e., moving behind the shock front from station (e) to (a), the two energy modes relax to an equilibrium state. The relaxation first starts in the core region of the tube and within a width of about 0.57 cm behind the shock (i.e., station (a)), the two energy modes
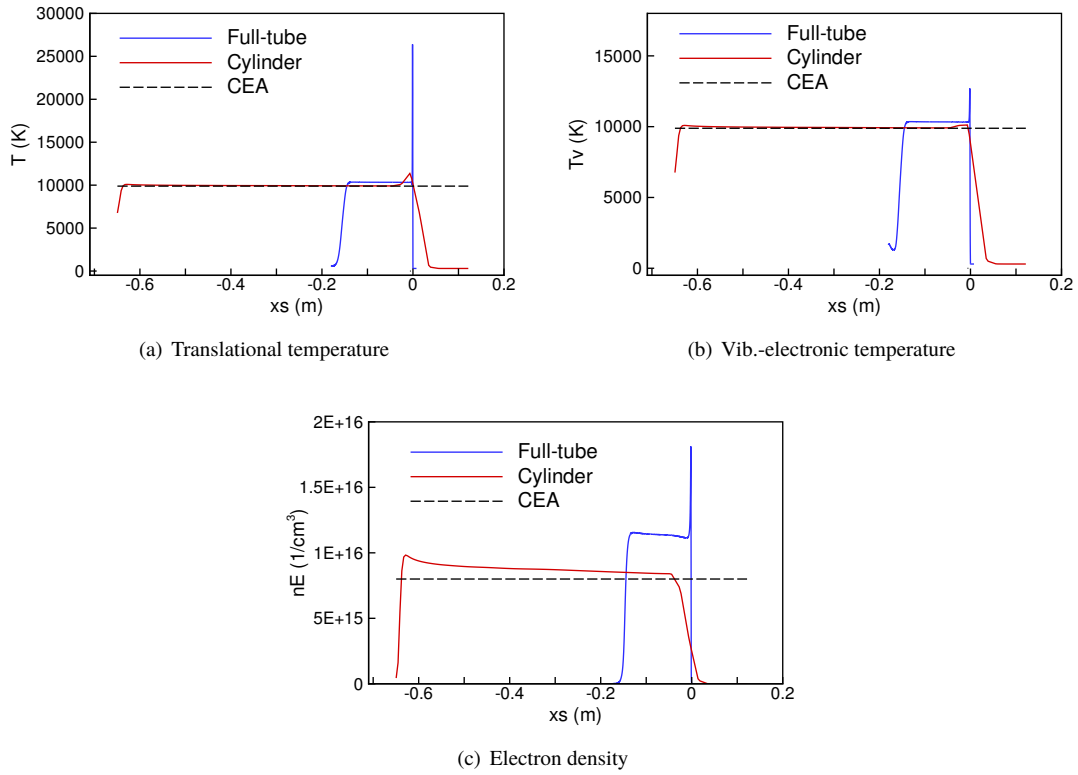
---

*https://www.grc.nasa.gov/www/CEAWeb/

(a) Translational temperature

(b) Vib.-electronic temperature

(c) Electron density

Fig. 4   Axial profiles for 10 km/s shock, xs = 0 represents the shock front location in the shock-frame of reference

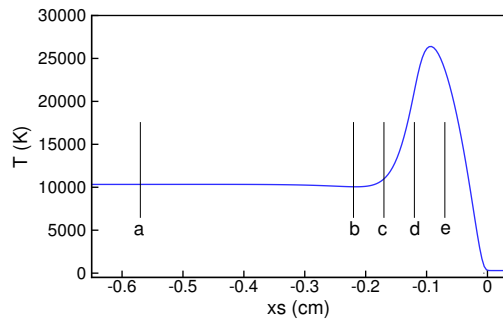

Fig. 5   Centerline temperature in the nonequilibrium region, LOS data is extracted at axial locations (a) - (e)
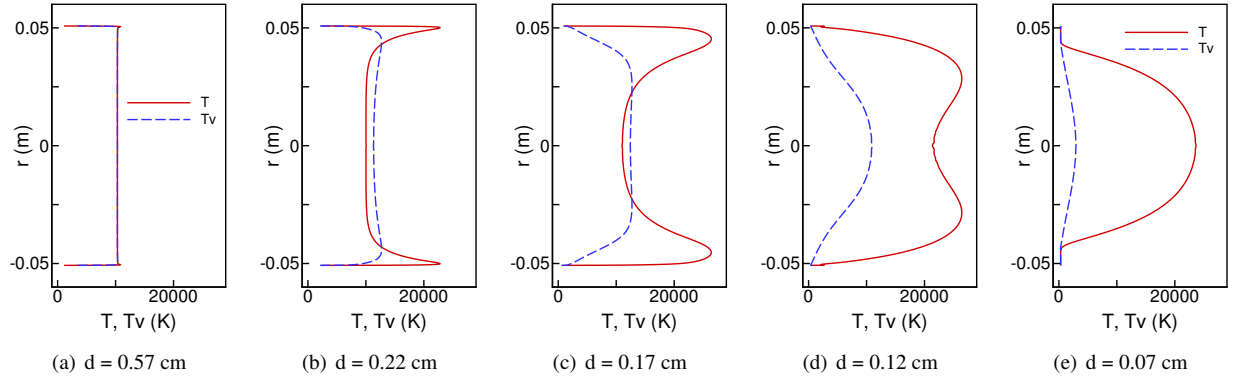
(a) d = 0.57 cm   (b) d = 0.22 cm   (c) d = 0.17 cm   (d) d = 0.12 cm   (e) d = 0.07 cm

Fig. 6   Radial temperature profiles in the nonequilibrium region, d is the distance behind the shock

(a) Shock deceleration along the tube   (b) Behavior near the test-section
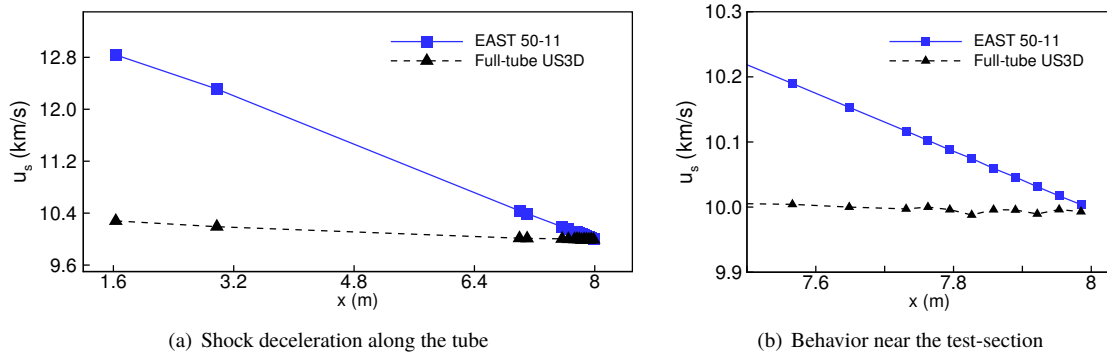
Fig. 7   Shock deceleration in EAST vs. US3D predictions

achieve a fair equilibrium in the near-wall region as well.

The shock deceleration profiles predicted by the full-tube US3D simulations are compared against the measured values in EAST shot no. T50-11 (10.01 km/s, 0.2 Torr). Fig. 7 shows the instantaneous shock velocity as the shock front is detected at various locations along the tube length. The shock speed in test is significantly higher than the predicted values until 6+ m of shock travel. The nonequilibrium effects caused by the shock deceleration cannot be fully represented.

B. Radiative Predictions

The radiation calculations are performed using the symmetry line data from the cylinder and the full-tube simulations described in the previous section. These flow field inputs are used in the Shock Tube (ST) mode in NEQAIR, in which the flow parameters at the tube centerline are assumed to be constant across the tube diameter. However, it is clear from the Fig. 6 that the centerline values can be significantly different from the near-wall values. Therefore, an additional NEQAIR simulation is performed in Line-Of-Sight (LOS) mode, using radial data information at various axial stations behind the shock.

The test-section in EAST shock tube is about 12 cm long in the axial direction. The integrated radiance in six different wavelength regimes from 130 - 1450 nm is plotted as a function of parameter d, which is the distance behind the shock (see Fig. 8). As expected, the full-tube radiance values are consistently higher than the cylinder based calculations, which is a result of the tube flow gas state converging to a non-CEA level higher than the CEA predicted equilibrium. Additionally, the full-tube based radiance from the LOS versus ST mode have significantly different features. The VUV radiance is lower in the ST mode than that in the LOS mode, indicating that the cold boundary layer is supporting the production of the species emitting in this spectral regime. Moreover, the peak radiance in 130 - 178 nm wavelength range, is about 2.5 times higher in LOS mode than that in ST mode. Such effects if not accounted for, can introduce large
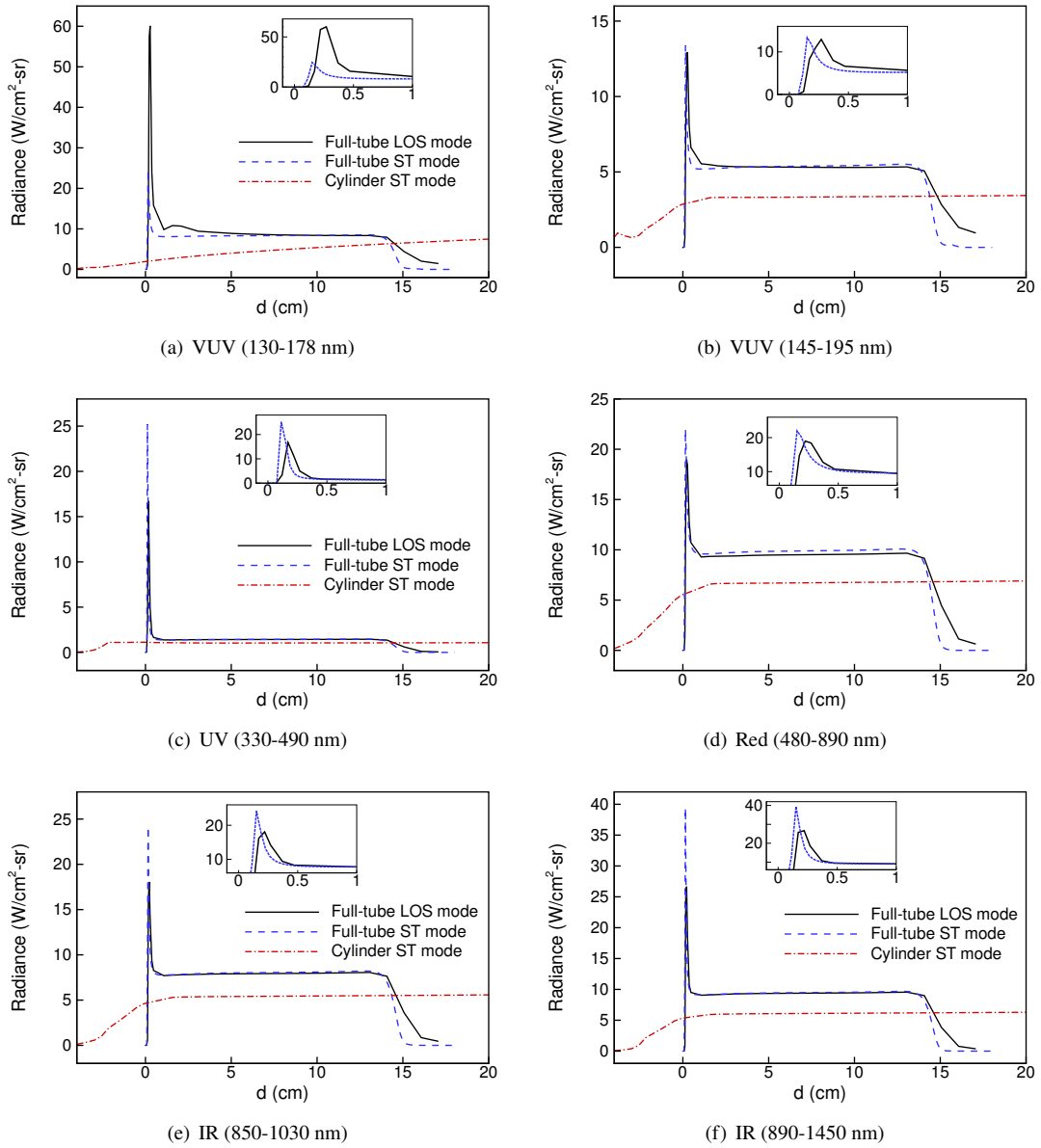
6

(a) VUV (130-178 nm)

(b) VUV (145-195 nm)

(c) UV (330-490 nm)

(d) Red (480-890 nm)

(e) IR (850-1030 nm)

(f) IR (890-1450 nm)

Fig. 8　Integrated radiance behind the shock using full-tube and cylinder based flow inputs

(a) VUV (130-178 nm)

(b) UV (330-490 nm)

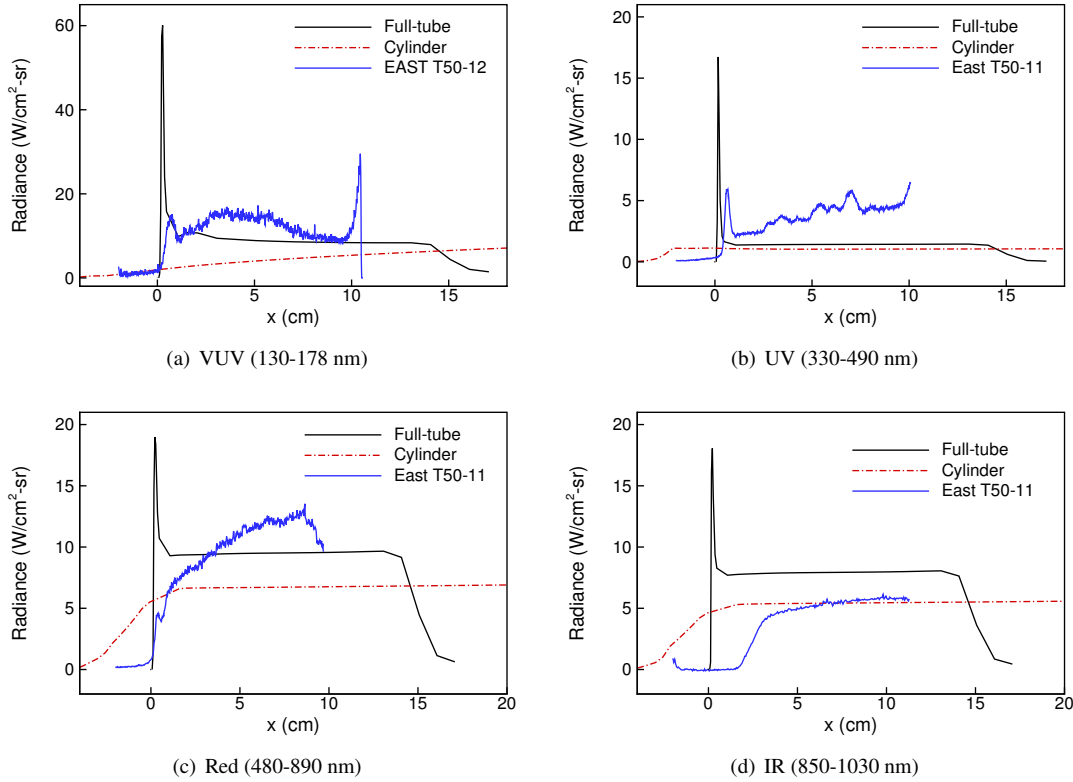(c) Red (480-890 nm)

(d) IR (850-1030 nm)

Fig. 9   Integrated radiance behind the shock validated against EAST data

errors in the surface heat-flux calculations. The differences in the LOS versus ST mode radiance predictions are seen in all other spectral regimes as well though they are less prominent than in the VUV regime. It is clear that the near-wall gas state and radiation properties are considerably different than that at the tube centerline. The full-tube simulations enable an accurate representation of the radial profiles which may improve the confidence in the radiative predictions.

C. Validation with EAST data

The previous section has indicated the importance of the LOS based radiative predictions. The radiation solver results are now directly compared with the experimental data as shown in Fig. 9. The EAST shots no. T50-11 (10.01 km/s) and T50-12 (10.04 km/s) at 0.2 Torr ambient pressure in air (79% N_2 + 21% O_2) are chosen to validate the current numerical predictions in four different spectral regimes from 130 - 1030 nm. The full-tube LOS based integrated radiance is plotted along with cylinder ST mode predictions and the measured values in test.

In all four regimes, the full-tube based peak radiance at the shock front is much higher than that reported in the test. This is not surprising as this peak is smeared in test data due to a relatively coarse spatial resolution used in the measurements. The radiance predictions from a realistic full-facility based flow field show a good agreement with the test data in the VUV spectral regime which is dominated by the electromagnetic emissions from the atomic species such as N at 174 nm. Interestingly, the high VUV radiance towards the contact front cannot be captured with current full-tube predictions. Moreover, the UV spectral region which mainly features diatomic excitations such as of N_2 and N_2^+ etc., is under-predicted by both, the full-tube and the cylinder based calculations, and the nonequilibrium test behavior is not captured.

Another interesting spectral region is the Red (480 - 890 nm) which is most affected by the shock deceleration effects present in the tube. The measured radiance increases significantly behind the shock and the cylinder based values show a large under-prediction of the test with a maximum error of about 65%. The full-tube predictions show some improvement in this region as they capture the shock deceleration effects up to some extent. The maximum error is reduced to about 25% by using the full-tube flow field in LOS mode. The Red region along with the IR regime features

the monoatomic excitation of N, O, etc. The post-shock behavior in IR region is better captured by the cylinder based flow field while the full-tube simulations show a over-prediction of about 30%.

It should be noted that the increment in the measured radiance behind the shock is much more prominent in the VUV to Red spectral regions whereas the full-tube based radiance profile is relatively flat for all four regimes. Thus, the full facility based flow field shows improvement in some parts of the EAST spectrum of interest but the influence of the boundary layer on the shocked gas state is not captured completely.

V. Summary

Radiative predictions are presented for lunar return Earth entry conditions. The shocked gas flow properties are computed in US3D flow solver and fed as an input to NEQAIR. The radiation calculations are performed using the shocked gas state behind a blunt-body geometry and at the EAST test-section for a full facility 2D-axisymmetric simulation. The cylinder flow field shows a CEA equilibrium state behind the shock as expected, whereas the post-shock state just behind the shock front reaches an equilibrium state significantly different than CEA predictions. This behavior is possibly caused by the rapid stretching of the grid cells in the axial direction and needs to be investigated further. However, the full-tube flow captures the radial variation in the gas properties due to the boundary layer effects. This data is used in the Line-Of-Sight (LOS) and the Shock Tube (ST) modes for computing the integrated radiance. The numerical predictions are then compared with the test data in four spectral regimes from VUV to IR. Some parts of the VUV and Red spectral regions show a better match with the test data when the full-tube flow field is used as an input. However, the UV and IR regions are under- and over-predicted respectively, and the nonequilibrium test behavior is not captured completely. The full-tube simulations used in current study are the first high-fidelity predictions of the full EAST facility and show promising improvements as compared to previously used blunt-body flow field for the interpretation of EAST data. Further modifications are required in the facility based simulations to address two important issues, 1) the post-shock equilibrium state being different from CEA predicted equilibrium, and 2) the shock deceleration being much smaller than that observed in the test.

VI. Future work

The numerical predictions presented here have shown some consistency with the test data while the nonequilibrium effects in all spectral regimes are not yet captured completely. The progress shown in current work is a good start but the ultimate goal of the full facility characterization of the EAST shock tube requires improvements at various levels.

The shock deceleration in the current full-tube simulations is significantly lower than the test. This can be possibly attributed to the rapid axial stretching of the grid just after a 2 cm wide region of heavey refinement while the shocked gas region is about 15-17 cm wide. Since the grid resolution affects the numerically predicted speed of discontinuities, the relatively coarser grid behind the shock can introduce errors in the gas speed predictions. More simulations will be performed to obtain an optimal grid resolution in the entire shocked gas region. It will be useful to simulate an 11 km/s air shock with the optimal grid for assessing the post-shock equilibrium as the test data at these conditions shows excellent equilibrium characteristics. Moreover, the current tube simulations model an idealized version of actual shock tube facility without any imperfections caused by the optical access windows, instrumental ports etc. The initial diaphragm breaking process is assumed to be instantaneous and smooth and radiative cooling is not considered. All these factors can affect the shock deceleration and a sensitivity study of these parameters may explain the differences between the test and the numerical predictions. New blunt-body simulations will be performed with better grid resolution. The flow field and radiative properties will be compared with that for full-tube simulations. A detailed analysis of the measured vs. numerically predicted radiation spectra will be performed in various wavelength regimes. This will provide a better understanding of the key phenomena and identify the missing ones in the current simulations. The nonequilibrium effects in the test are more prominent for the moderate Earth entry speeds less than 10 km/s. Additional simulations will be performed for 8 and 9 km/s Earth entry at 0.2 Torr – the flow and radiative predictions will be compared against the test to identify any further discrepancies in the numerical predictions.

The improved simulation approach from above steps will be used to simulate and validate Mars entry conditions at 6.25 km/s, 0.25 Torr. The importance of afterbody raditive predictions for high speed Earth entry capsules was elucidated by Johnston & Brandis [4]. In order to accurately compute the radiation field in the afterbody region, high-fidelity CFD simulations for the expanding shocked-gas will be performed with the US3D flow solver. The flow field obtained will be used for the radiation calculations. The overall objective is to provide accurate heating predictions for a range of Earth entry missions tested in EAST. Additional simulations at various atmospheric conditions will

be performed to cover the upper range of the operational envelope for Earth entry and numerical predictions will be compared against test data. This analysis will provide an assessment of current predictive capability and will open pathways for further improvements in the numerical set-up.

Acknowledgments

References

[1] Brandis, A. M., Johnston, C. O., Cruden, B. A., and Prabhu, D., "Validation of High Speed Earth Atmospheric Entry Radiative Heating from 9.5 to 15.5 km/s," AIAA-2012-2865, June 2012.

[2] Thomas K., W., Theisinger, J. E., Brune, A. J., and Johnston, C. O., "Backshell Radiative Heating on Human-Scale Mars Entry Vehicles," AIAA-2017-4532, June 2017.

[3] Brandis, A. M., Saunders, D. A., Johnston, C. O., Cruden, B. A., and White, T. R., "Radiative Heating on the After-Body of Martian Entry Vehicles," AIAA-2015-3111, June 2015.

[4] Johnston, C. O., and Brandis, A. M., "Features of Afterbody Radiative Heating for Earth Entry," *Journal of Spacecraft and Rockets*, Vol. 52, No. 1, Dec. 2015, pp. 105–119.

[5] Brandis, A. M., Cruden, B. A., Prabhu, D., Bose, D., McGilvray, M., and Morgan, R. G., "Analysis of Air Radiation Measurements Obtained in the EAST and X2 Shocktube Facilities," AIAA-2010-4510, June 2010.

[6] Kotov, D. V., Yee, H. C., Panesi, M., Prabhu, D. K., and Wray, A. A., "Computational Challenges for Simulation related to the NASA Electric Arc Shock Tube (EAST) Experiments," *Journal of Computational Physics*, Vol. 269, July 2014, pp. 215–233.

[7] Cruden, B. A., "Electron Density Measurement in Reentry Shocks for Lunar Return," *Journal of Thermophysics and Heat Transfer*, Vol. 26, No. 2, June 2012, pp. 222–230.

[8] Chandel, D., Nompelis, I., and Candler, G. V., "Numerical Simulation of Propagation of Strong Shock Waves," AIAA-2017-0744, Jan. 2017.

[9] Chandel, D., Nompelis, I., and Candler, G. V., "Computations of High Enthalpy Shock Propagation in Electric Arc Shock Tube (EAST) at NASA Ames," AIAA-2018-1722, Jan. 2018.

[10] Cruden, B. A., "Absolute Radiation Measurements in Earth and Mars Entry Conditions," RTO-EN-AVT-218, 2014.

[11] Brandis, A. M., Johnston, C. O., Cruden, B. A., Prabhu, D., and Bose, D., "Uncertainty Analysis and Validation of Radiation Measurement for Earth Reentry," *Journal of Thermophysics and Heat Transfer*, Vol. 29, No. 2, 2015, pp. 209–221.

[12] Brandis, A., and Cruden, B. A., "Benchmark Shock Tube Experiments of Radiative Heating Relevant to Earth Re-entry," AIAA-2017-1145, Jan. 2017.